Neutron diffraction investigation of an in-plane biaxial fatigued stainless steel sample of cruciform geometry

2008 J. Phys.: Condens. Matter 20 104257

(http://iopscience.iop.org/0953-8984/20/10/104257)

IOP Publishing Journal of Physics: Condensed Matter

J. Phys.: Condens. Matter **20** (2008) 104257 (6pp) doi:10.1088/0953-8984/20/10/104257

Neutron diffraction investigation of an in-plane biaxial fatigued stainless steel sample of cruciform geometry

Yu V Taran[1,5], A M Balagurov[1], S G Sheverev[1], J Schreiber[2], A M Korsunsky[3], W J J Vorster[3], H Bomas[4] and C Stoeberl[4]

[1] Frank Laboratory of Neutron Physics, Joint Institute for Nuclear Research, Dubna, Russia
[2] Fraunhofer Institute for Nondestructive Testing (Dresden branch), Germany
[3] Department of Engineering Science, University of Oxford, UK
[4] Division of Material Science, Foundation Institute for Materials Science, Bremen, Germany

E-mail: taran@nf.jinr.ru

Received 2 July 2007, in final form 15 November 2007
Published 19 February 2008
Online at stacks.iop.org/JPhysCM/20/104257

Abstract

Fatigue and fracture under multiaxial stresses are among the most important current research topics aimed at ensuring improved reliability of industrial components. An *ex situ* in-plane biaxial low cycle fatigued sample of cruciform geometry from austenitic stainless steel AISI 321 H was investigated on the FSD stress-diffractometer at the IBR-2 pulsed nuclear reactor by using the neutron strain scanner and the uniaxial stress rig. The phase composition of fatigued material was determined and the residual macrostresses and phase microstresses were measured. To the best of our knowledge, no neutron diffraction investigations of materials subjected to biaxial loading have been previously carried out. The first results of the neutron diffraction experiment are presented and discussed.

1. Introduction

During fatigue loading of structural materials changes occur in the microstructure which affect the mechanical and physical properties. The experimental simulation of these changes can be performed by cyclic mechanical loading, usually in the form of uniaxial tension–compression fatigue cycling. However, machines and structures are frequently subjected to complex multiaxial stresses. Prediction of failure under multiaxial stresses is one of the most important remaining challenges to ensuring the reliability of industrial components. Conventional uniaxial load tests in combination with classical yield criteria often fail to predict adequately in-service fatigue failures [1]. Design engineers require improved tools for the evaluation of strength and reliability of materials under multiaxial loading conditions. The field of multiaxial stress testing covers a range of experimental techniques using various specimen geometries, e.g. in-plane biaxial or coaxial tension–torsion fatigue.

The behaviour of several structural materials is of interest in this context, e.g. stainless steels, duplex-phase steels, shape-memory alloys, etc. Low carbon titanium-stabilized chrome–nickel austenitic stainless steel (ASS) of AISI 321 type is of special interest due to its outstanding properties, such as high corrosion resistance, excellent mechanical properties and weld ability. This type of steel is widely used in highly safety critical industries, for example, in the nuclear industry and nuclear power generation plants. However, a major problem in a number of applications is the mechanical property degradation due to martensite formation in ASS components under multiaxial loading fatigue. For these components the assessment of fatigue damage and of the remaining fatigue lifetime of material is a task of great practical importance.

Many investigations using conventional mechanical testing and radiation methods (x-ray- and neutron diffraction (ND)) show the influence of material processing history (founding, annealing, quenching, etc) and fatigue cycling conditions (load amplitude, frequency, stress or strain control, temperature, value of R-ratio, number of cycles, etc) on the fatigue properties of ASS. Due to its phase sensitivity, neutron diffraction offers a powerful tool for the investigation of fatigue properties of multiphase industrial materials. Such investigations have the capacity to extract qualitatively new

[5] Author to whom any correspondence should be addressed.

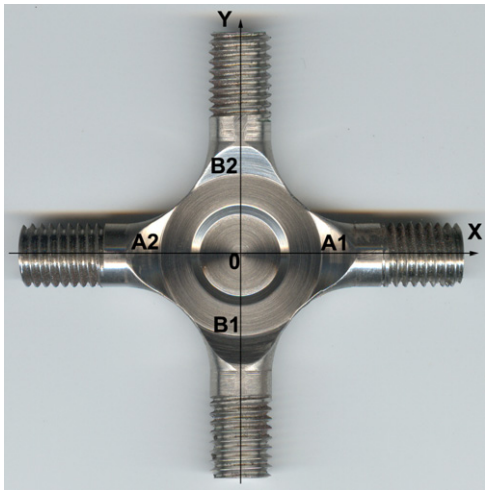

Figure 1. Sample Krest-2.
(This figure is in colour only in the electronic version)

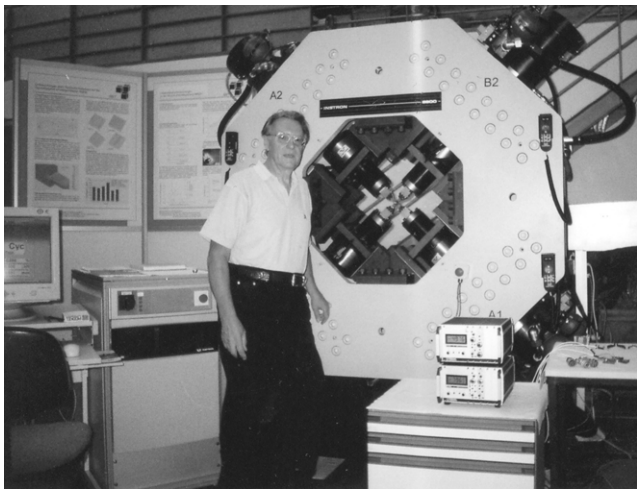

Figure 2. Instron 100 kN planar biaxial machine.

information on the properties of multiphase materials that cannot be obtained by the conventional methods.

ND investigations have previously been carried out by our group on steel AISI 321 subjected to uniaxial low and high cycle fatigue (LCF/HCF) loading on ENGIN and ENGIN-X stress-diffractometers at the ISIS neutron pulsed facility [2–8]. When the transition is made from uniaxial to in-plane biaxial cycling, residual stress distribution becomes spatially varying and therefore more complicated. The present work describes the *ex situ* in-plane biaxial fatigue mechanical testing of a sample of cruciform geometry from AISI 321 steel and *in situ* neutron diffraction stress analysis of the fatigued sample performed on the FSD time-of-flight stress-diffractometer at the IBR-2 nuclear pulsed reactor (Dubna).

2. Experimental details

The material examined was a low carbon Ti-alloyed metastable austenitic stainless steel of the Russian grade 12X18H10T (which is an analogue of the US grade AISI 321 H). The steel was delivered in the form of hot-rolled sheet with the thickness of 16 mm. The chemical composition is presented in table 1. The yield stress $R_{p0.2}$ and the tensile strength R_m were defined by the producer to be equal to 370 MPa and 580 MPa, respectively.

The cruciform sample designated Krest-2 (figure 1) was subjected to in-plane biaxial fatigue cycling up to 407 cycles at the frequency of 0.5 Hz and the applied load of 17 kN on the INSTRON planar biaxial loading machine (figure 2). Two possible cycling modes were considered: in-phase load (tension–compression along both axes) and out-of-phase load (tension–compression along one of the axes and compression–tension along a second axis). The latter was chosen for the present investigation.

To measure the radial variation of residual strains in the austenite matrix and martensite precipitates the sample of Krest-2 was installed on the neutron strain scanner. Two detectors at scattering angles of $\pm 90°$ were used for simultaneous measurement of neutron diffraction spectra in one of two planar and transverse directions of the neutron scattering vector, respectively. Both detectors consisted from geometry focused ZnS sections. Spectra from different sections of each detector were 'focused' electronically. One of the detectors was equipped with the multi-slit focused radial collimator providing 2 mm spatial resolution. The sample central part had the form of a 2 mm thick membrane of 15 mm diameter. Both detectors measured lattice parameters averaged across the entire membrane thickness. Diffraction spectra contained eight austenitic and six martensitic reflections in the d-spacing range between 0.8 and 2.1 Å. The spectra were processed by the Rietveld refinement method to obtain the phase lattice parameters a.

The four strain scans were performed along the A1–A2 and B1–B2 cycling directions (see figure 1). For brevity below these directions will be referred to as x- and y-axes, respectively. Each of these two directions were in turn arranged to be parallel to the scattering vector. Below we refer to the lattice parameters measured for each axis in the x- and y-directions of the scattering vector as the x- and y-components of a.

To investigate the mechanical response of the material (applied load versus phase-specific elastic strain responses), sample Krest-2 was mounted inside the portable electromechanical uniaxial load testing machine TIRA placed on the strain scanner. The x-axis of the sample was directed along the horizontal load axis that coincided with the scattering vector. The measurements were carried out with the detector without the radial collimator, and only one planar component of the phase lattice parameters was measured during *in situ* uniaxial loading in the stress rig.

3. Experimental results of the strain scanning

In figure 3, the results of planar strain scanning are presented as a radial distribution of the (x, y)-components of the lattice parameters for the austenite (left-hand side figure) and martensite (right-hand side figure). The data about

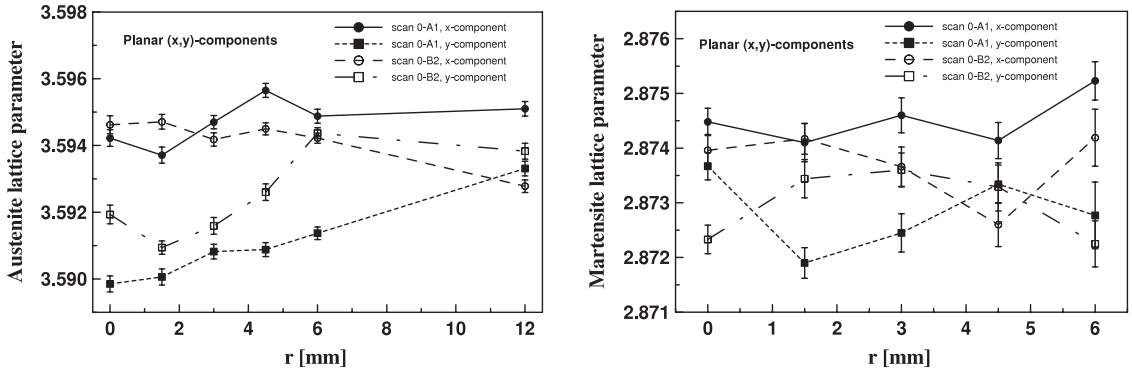

Figure 3. Radial dependence of the planar lattice parameter (Å): left—austenite, right—martensite.

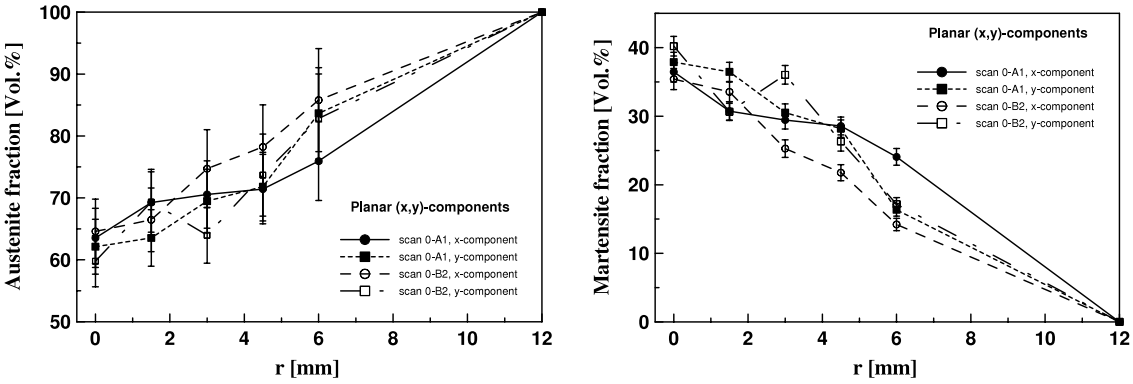

Figure 4. Radial dependence of the planar volume fraction: left—austenite, right—martensite.

Table 1. Chemical composition of the steel 12X18H10T.

Elements	C	Mn	Si	S	P	Cr	Ni	Ti	Mo	V	W
Weight-%	0.07	0.65	0.40	0.009	0.039	17.78	9.41	0.42	0.09	0.05	0.03

the austenite and martensite volume fractions are shown in figure 4.

4. Phase a_0-problem

Since the austenite matrix volume fraction is appreciably reduced during fatigue cycling, while the martensite phase is created in the same process, it is not possible in principle to obtain stress-free reference samples of these phases in order to estimate the residual strains and then the corresponding stresses. One opportunity at our disposal to make such estimations was to use the value of the austenite lattice parameter derived from the measurements made on the sample 'legs' where plastic deformation has not taken place, and no martensite has been created (see figure 4, right-hand end). The other option is to use the stress equilibrium approach reviewed in [9] to obtain the martensite a_0-lattice parameter. We note the approximate nature of the approach used in the present study.

4.1. Austenite matrix

As seen in table 2, the results of the four separate measurements of the austenite lattice parameters on sample 'legs' lie within the 98% confidence interval, providing the basis for evaluating the austenite a_0-value as their average equal to 3.593 75(50) Å.

Table 2. Austenite lattice parameters from sample 'legs'.

Axis	x-component of a (Å)	y-component of a (Å)
0-A1 direction	3.595 10(22)	3.593 31(22)
0-B2 direction	3.592 78(19)	3.593 83(24)

4.2. Martensite inclusions

According to [9], the phase total residual stress is the sum of the macrostress and the phase microstress:

$$\langle {}^t\sigma_j^p \rangle = {}^M\sigma_j + \langle {}^\mu\sigma_j^p \rangle, \tag{1}$$

where the angle brackets indicate that the stresses are averaged over the gauge volume (hereinafter, they will be omitted for short), the superscripts M and μ denote, respectively, the macrostress that is the same in each phase, and the microstress in the p-phase, where superscript p takes the values of a

for austenite and m for martensite, respectively. Subscript j indicates the stress component at a sampled point. Each macrostress component must average to zero over the entire volume of the body:

$$^{M}\bar{\sigma}_j = \frac{1}{V}\int_V {}^{M}\sigma_j \, \mathrm{d}V = 0. \tag{2}$$

Furthermore, within each representative volume element (RVE) microstress components must sum to zero when weighted by their volume fraction:

$$^{\mu}\sigma_j^a f^a + {}^{\mu}\sigma_j^m f^m = 0, \tag{3}$$

where f^a and f^m represent the volume fraction of austenite and martensite, respectively ($f^a + f^m = 1$, since no other phases are assumed to be present). Using (1)–(3), the macrostress and the phase microstress may be determined as follows:

$$^{M}\sigma_j = {}^{t}\sigma_j^a f^a + {}^{t}\sigma_j^m f^m \tag{4}$$

$$^{\mu}\sigma_j^a = f^m({}^{t}\sigma_j^a - {}^{t}\sigma_j^m) \tag{5}$$

$$^{\mu}\sigma_j^m = -f^a({}^{t}\sigma_j^a - {}^{t}\sigma_j^m). \tag{6}$$

Substituting (4) into (2) and taking into account that the measurements were made at n positions along the i-axis (where i may be associated with x or y), the integral in (2) is transformed into a sum:

$$\sum_{i=x}^{y}\sum_{k=1}^{n}[{}^{t}\sigma_j^a(x_{i,k}) f_j^a(x_{i,k}) + {}^{t}\sigma_j^m(x_{i,k}) f_j^m(x_{i,k})] = 0, \tag{7}$$

where the coordinate $x_{i,k}$ corresponds to the kth point along the i-axis.

Total phase stresses in the membrane part of the sample are assumed to be planar (plane stress condition). In this case triaxial Hooke's law is reduced to biaxial representation and expressed through the phase lattice parameter $a_{i,x(y)}$ at position $x_{i,k}$ (the phase index is omitted):

$${}^{t}\sigma_x(x_{i,k}) = \frac{E}{1-\nu^2}\left[\frac{a_{i,x}(x_{i,k}) + \nu a_{i,y}(x_{i,k})}{a_0} - (1+\nu)\right] \tag{8}$$

$${}^{t}\sigma_y(x_{i,k}) = \frac{E}{1-\nu^2}\left[\frac{\nu a_{i,x}(x_{i,k}) + a_{i,y}(x_{i,k})}{a_0} - (1+\nu)\right]. \tag{9}$$

Assuming that there is no elastic property mismatch between the phases and substituting (8) and (9) into (7), the martensite a_0-values were calculated to be equal to 2.87405 and 2.870 34 Å for $j = x$ and y, respectively. The mean of these values, 2.872 20 Å, will be used as the martensite a_0-value for strain calculations.

5. Residual stress calculations

The planar total residual stress components of both phases into the sample membrane are shown in figures 5 and 6. The austenite bulk value of $E = 170$ GPa and $\nu = 0.3$ was determined from uniaxial loading experiments. The same elastic constants were used for the martensite phase under the assumption of lack of elastic stiffness mismatch between the phases. It is apparent from the figures that compression in the austenite phase is balanced by tension in the martensite phase.

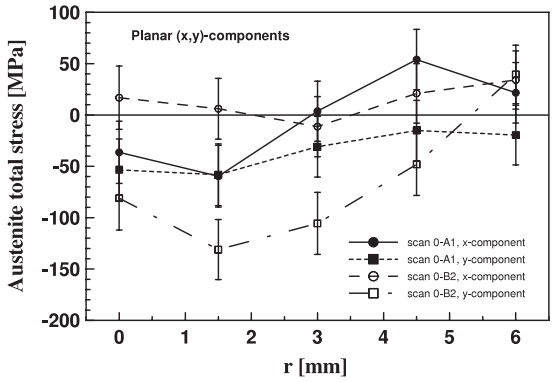

Figure 5. Radial dependence of the planar total residual stress components of austenite.

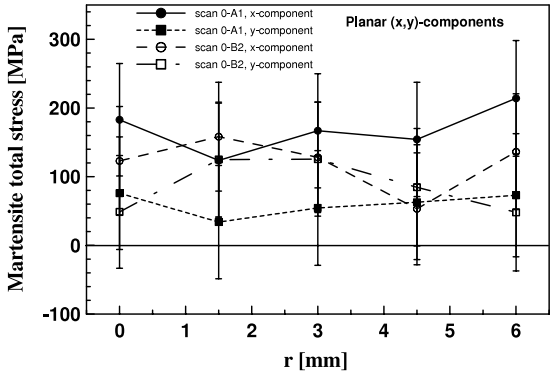

Figure 6. Radial dependence of the planar total residual stress components of martensite.

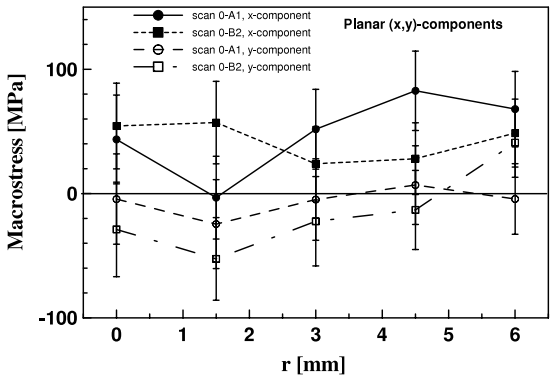

Figure 7. Radial dependence of the planar macrostress components.

According to equations (4)–(6), in two-phase materials it is possible to determine both the macrostresses in the material and the average microstresses present in each phase. The results of such separation of phase total residual stresses into macrocomponents and microcomponents are shown in figures 7 and 8.

Since the sample membrane was irradiated through its thickness by the neutron beam, only the planar residual

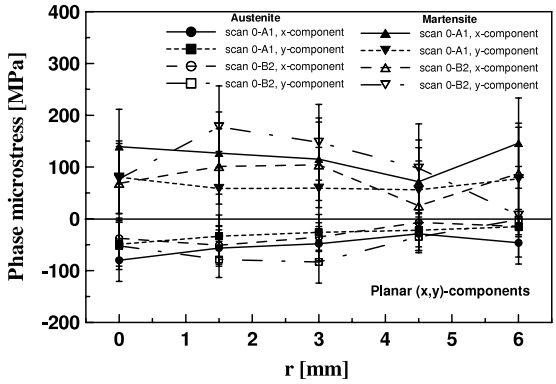

Figure 8. Radial dependence of the planar phase microstress.

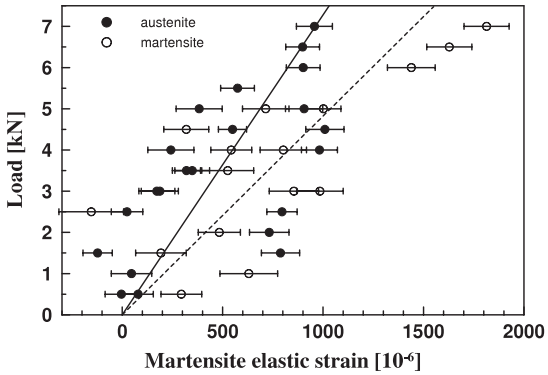

Figure 9. Applied load–elastic strain responses of the austenite and martensite.

macrostress components were expected to differ from zero (figure 7). Indeed, their values approach the level of experimental error. To make a backward check of feasibility of equation (7) in our case, each macrostress component was averaged over all measured points on both scan axes. The results of averaging were as follows: ${}^{M}\bar{\sigma}_x = 45(32)$ MPa, ${}^{M}\bar{\sigma}_y = -11(33)$ MPa. The fact that the average residual macrostresses were not equal to zero indicates the approximate nature of the assumptions made in our analysis and the procedure for the determination of phase-specific stress-free lattice parameters. This observation particularly concerns the calculation of martensite a_0-value, when integration over the sample volume was replaced with simple summation along the scanning lines. Nevertheless, the result of macrostress separation is satisfactory in view of the limited precision of experimental data.

The results of separation of the planar phase microstress components (figure 8) show that the austenite phase found itself in compression, while the martensite phase exhibited a balancing tensile stress with the larger value, in accordance with its smaller volume fraction. This result requires further elucidation. The martensite formation is connected with volume increase (dilatation). Since the specific volume of martensite is larger (by about 2%) than that of austenite, the martensite phase is generally expected to be in hydrostatic compression, with austenite respectively being in tension. The present experimental results demonstrate the opposite sign for phase microstresses. This phenomenon, however, has already been observed in uniaxial LCF samples of the same steel [5]. This effect was interpreted as the consequence of superposition of phase transformation stresses on the deformation stresses caused by plastic deformation during LCF. The interplay of these stresses creates the resulting phase residual stress that is not of purely hydrostatic nature, with deformation-induced stresses being overshadowed by phase transformation stresses. It is also worth noting that the rather large tensile microstresses observed in the martensite may promote crack initiation.

6. *In situ* uniaxial stress rig experiment

In situ uniaxial stress rig measurements were carried out to explore the relationship between applied load and elastic strain for austenite and martensite phases in sample Krest-2. The elastic region (loads below 7 kN) was considered, in order to preserve the residual stress distribution due to prior cycling for future investigations.

The experimental dependences of phase lattice parameters on the applied load were fitted with linear trend lines in order to obtain phase lattice parameters a_0 at zero load, and the slope B. The results were as follows: $a_{0,\mathrm{aus}} = 3.572\,85(14)$ Å and $B_{\mathrm{aus}} = 4.91(35) \times 10^{-4}$ Å kN^{-1}; $a_{0,\mathrm{mar}} = 2.855\,37(19)$ Å and $B_{\mathrm{mar}} = 5.91(44) \times 10^{-4}$ Å kN^{-1}. These phase-specific reference parameters a_0 differed from the true stress-free a_0-values due to small adjustment of diffractometer configuration (removal of radial collimator and installation of the stress rig). However, it was not thought necessity to re-calibrate the diffractometer to calculate the responses.

Using phase-specific a_0-parameters the applied load–elastic strain responses of the austenite and martensite phases were calculated (figure 9). This figure appears to indicate an elastic stiffness mismatch between phases illustrated by the lines of a linear fit to the data constrained to pass through zero. However, the result must be considered with care due to strong scatter in the experimental points, and low reproducibility of strain measurements. Note that the moderate elastic mismatch between the austenite and martensite phases was firstly observed in the uniaxial high cycle fatigued samples of same steel [10]. However, the uniaxial low cycle fatigued samples did not reveal any elastic stiffness mismatch between the austenite and martensite phases [11].

More precise and reliable measurements of applied load–elastic strain responses for both phases in the in-plane biaxial low cycle fatigued sample of cruciform geometry are necessary. Reliable gripping of the sample in the testing machine and precise control of the location of thin sample membrane in the neutron beam are crucial here.

A rough estimate of the martensite Young's modulus E may be made using the phase slope B expressed through a_0 (Å), E (GPa) and the effective cross-section S_{eff} (cm^2) of the load applied to the membrane: $B = a_0/(100 E S_{\mathrm{eff}})$. Using the austenite modulus E of 170 GPa measured during the quasistatic uniaxial testing on the Instron machine, the effective cross-section S_{eff} was found to be

equal to 0.43(3) cm^2 compared to the geometrical cross-section S_{geo} of the membrane in the sample centre equal to 0.2 cm × 1.5 cm = 0.3 cm^2. The martensite Young's modulus was estimated to be equal to 112(17) GPa using the effective cross-section S_{eff} obtained for the austenite phase.

7. Conclusion

The in-plane biaxial low cycle fatigued sample of the cruciform geometry from a low carbon Ti-alloyed metastable austenitic stainless steel of the Russian grade GOST 12X18H10T (an analogue of the US grade AISI 321 H) was investigated on the FSD Fourier time-of-flight neutron stress-diffractometer at the IBR-2 pulsed nuclear reactor (Dubna). To the best of our knowledge, no neutron diffraction investigations of materials subjected to biaxial loading have been previously carried out.

The lattice parameters in the austenite matrix and the martensite inclusions created during the fatigue cycling, as well as the martensite volume fraction, were measured along two mutually perpendicular planar axes of the sample. The martensite fraction changes from 38% in the sample centre to 18% at the membrane circumference.

Phase total residual strain/stress components were calculated from the experimental data using the phase stress-free lattice parameters a_0. The austenite a_0-value was measured into two of the four 'legs' of the sample, where the plastic deformation during fatigue cycling was small, and no appreciable martensite volume fraction could be expected. The martensite a_0-value was calculated from the experimental data using the austenite a_0-value and stress equilibrium relations.

The separation of phase total stresses into the residual macrostresses and microstresses was performed using the rule of mixtures. The macrostresses were small and were comparable with the experimental error. The calculation of the microstresses has shown that the austenite phase was in residual compression, while the martensite phase was in a balancing residual tension with the larger value in accordance with the smaller volume fraction.

The measurements of the applied load–phase elastic strain responses in the elastic region were carried out at the membrane centre using the TIRA uniaxial load machine. The effective cross-section of the load application on the sample membrane was determined from the austenite response with help of the previously measured austenite elastic modulus. The martensite elastic modulus was calculated from the corresponding strain response using the effective cross-section determined from the austenite response. The martensite modulus appears to be strongly different from that of the austenite. This result seems to indicate a large elastic mismatch between the two phases. However, it is necessary to consider this result with particular care due to low reproducibility of phase response measurements.

References

[1] Lohr R 2001 System design for multiaxial high-strain fatigue testing *ASTM STP* **1387** 355
[2] Daymond M R, Schreiber J and Taran Yu V 2001 *J. Neutron Res.* **9** 207
[3] Taran Yu V, Daymond M R, Eifler D, Nebel Th and Schreiber J 2002 *Mater. Sci. Forum* **404–407** 501
[4] Taran Yu V, Daymond M R and Schreiber J 2003 *J. Neutron Res.* **11** 4255
[5] Taran Yu V, Daymond M R and Schreiber J 2004 *Physica* B **350** 98
[6] Taran Yu V, Daymond M R, Eifler D, Nebel Th and Schreiber J 2005 *Mater. Sci. Technol.* **21** 35
[7] Taran Yu V, Daymond M R, Oliver E C and Schreiber J 2006 *Z. Kristallogr.* (Suppl. 23) 345–50
[8] Taran Yu V, Daymond M R, Schreiber J and Oliver E C 2006 *Mater. Sci. Forum* **524/525** 899
[9] Winholtz R A 1992 Separation of microstresses and macrostresses *Measurements of Residual and Applied Stress using Neutron Diffraction* ed M T Hutchings and A D Krawitz (Dordrecht: Kluwer–Academic) pp 131–45
[10] Taran Yu V, Daymond M R and Schreiber J 2002 *Appl. Phys.* A **74** (Suppl.) S1385–7
[11] Taran Yu V, Daymond M R, Eifler D and Schreiber J 2002 *Appl. Phys.* A **74** (Suppl.) S1391